Inactivation Defects Caused by Myotonia-associated Mutations in the Sodium Channel III–IV Linker

LAWRENCE J. HAYWARD,* ROBERT H. BROWN, JR.,* and STEPHEN C. CANNON*‡

From the *Department of Neurology, Massachusetts General Hospital, Boston, Massachusetts 02114; and ‡Department of Neurobiology, Harvard Medical School, Boston, Massachusetts 02115

ABSTRACT Missense mutations in the skeletal muscle Na^+ channel α subunit occur in several heritable forms of myotonia and periodic paralysis. Distinct phenotypes arise from mutations at two sites within the III–IV cytoplasmic loop: myotonia without weakness due to substitutions at glycine 1306, and myotonia plus weakness caused by a mutation at threonine 1313. Heterologous expression in HEK cells showed that substitutions at either site disrupted inactivation, as reflected by slower inactivation rates, shifts in steady-state inactivation, and larger persistent Na^+ currents. For T1313M, however, the changes were an order of magnitude larger than any of three substitutions at G1306, and recovery from inactivation was hastened as well. Model simulations demonstrate that these functional differences have distinct phenotypic consequences. In particular, a large persistent Na^+ current predisposes to paralysis due to depolarization-induced block of action potential generation. Key words: muscle • paralysis • familial • ion channels • human

INTRODUCTION

Voltage-gated Na^+ channels mediate action potential generation and conduction. Several dominantly inherited diseases of muscle excitability arise because of missense mutations in the human skeletal muscle Na^+ channel, hSkM1 (reviewed in Rüdel et al., 1993). Electrophysiologic studies have shown that many of these mutations prevent the normal fast inactivation of Na^+ channels (Cannon et al., 1991; Cannon and Strittmatter, 1993; Chahine et al., 1994; Lerche et al., 1993; Mitrovic et al., 1994; Mitrovic et al., 1995; Yang et al., 1994). The resulting persistent Na^+ current may cause repetitive action potentials (myotonia) or sustained depolarization and block of further contraction (Cannon and Corey, 1993).

The muscle disorders associated with Na^+ channel mutations have been grouped into three clinical phenotypes. Hyperkalemic periodic paralysis (HyperPP)[1] is characterized by episodic weakness caused by muscle depolarization. The weakness may be severe and generalized, although it largely spares respiratory function. Attacks of HyperPP are usually associated with mild elevation of serum $[K^+]$ (4.5–8 mM) and may be triggered by rest after exercise, cold, hunger, or oral K^+ loading (Riggs, 1988). In some families with HyperPP, myotonia may be present either clinically, as muscle stiffness, or on electromyographic testing. Strength is normal between attacks. In paramyotonia congenita (PMC), myotonic muscle stiffness paradoxically worsens with repetitive muscle activity. Cooling also aggravates the myotonia in PMC. With prolonged cooling, PMC muscle may depolarize and cause weakness. Sodium channel myotonia (SCM) is characterized by myotonia without weakness. Muscle stiffness may be constant or exacerbated by K^+ loading or rest after exercise (Rüdel et al., 1993).

At least 14 different missense mutations in the hSkM1 gene on chromosome 17q have been documented in families with these disorders (Rüdel et al., 1993). This gene encodes a pore-forming 260-kD protein, the α subunit, which in combination with an accessory 38-kD β_1 subunit forms the skeletal muscle sodium channel (Kraner et al., 1985). The four homologous domains (I–IV) of the α subunit each consist of six transmembrane segments and associated cytoplasmic and extracellular loops (Fig. 1), but the fine structure of these elements has not been established. Biochemical modifications and site-directed mutagenesis have delineated specific functions for subregions of the α subunit. This approach has highlighted certain components such as the cytoplasmic linker between domains III and IV (Stühmer et al., 1989; West et al., 1992) as the probable fast inactivation gate envisioned by Armstrong and Bezanilla (1977) that occludes the ion-con-

Address correspondence to Stephen Cannon, EDR413, Massachusetts General Hospital, Boston, MA 02114. Fax: (617) 726-5256; E-mail: cannon@helix.mgh.harvard.edu

[1] *Abbreviations used in this paper:* HyperPP, hyperkalemic periodic paralysis; PMC, paramyotonia congenita; SCM, sodium channel myotonia; TTX, tetrodotoxin; WT, wild type.

 J. GEN. PHYSIOL. © The Rockefeller University Press • 0022-1295/96/05/559/18 $2.00
Volume 107 May 1996 559–576

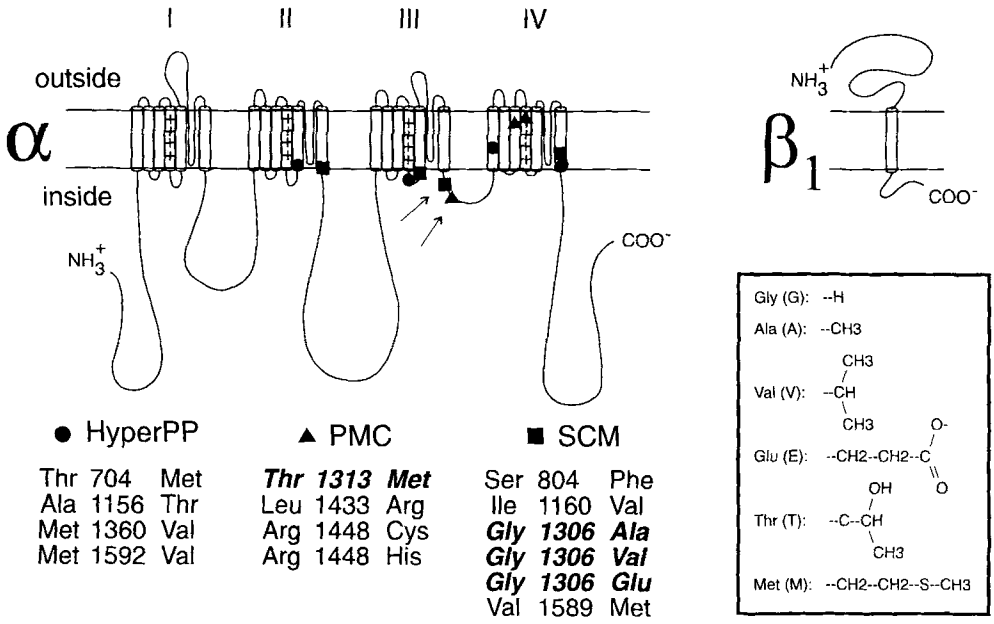

FIGURE 1. Schematic representation of skeletal muscle Na^+ channel subunits and the location of point mutations in HyperPP (●), PMC (▲), and SCM (■). The mutations characterized in this study (*italics*) are located by arrows, and their amino acid side chains and abbreviations are shown. Numbering of amino acid residues corresponds to homologous sites in human SkM1.

ducting pore within a few milliseconds after channel opening. In fact, 10 of the 14 mutations might be expected, a priori, to affect inactivation. Four mutations are within the III–IV linker itself, while another six mutations lie at the cytoplasmic ends of transmembrane segments 5 or 6, which may form a docking site for the inactivation particle at the inner vestibule of the channel pore. Knowledge of the specific biophysical defects caused by each mutation is required to correlate a particular location/substitution with functional effects that cause the corresponding clinical phenotype (HyperPP, PMC, or SCM).

In this study, we investigated the biophysical properties of disease mutations within the Na^+ channel III–IV linker. Mutations were engineered into the rat skeletal muscle α subunit cDNA (rSkM1, μl) corresponding to the human SCM disease mutations G1306A, G1306E, and G1306V, and a PMC mutation, T1313M (Fig. 1). rSkM1 is highly homologous to the human muscle Na^+ channel and has been shown to be suitable for expression of human disease mutations (Cannon and Strittmatter, 1993; Cummins et al., 1993; Chahine et al., 1994). These cDNAs were expressed transiently in HEK cells, and whole-cell Na^+ currents showed clear electrophysiological distinctions between SCM (residue 1306) and PMC (residue 1313) mutations. To estimate the functional consequences of a mutation upon muscle behavior, measured channel kinetics were incorporated into our mathematical model of a muscle cell (Cannon et al., 1993). Model simulations demonstrate that the different forms of inactivation defect observed in these mutants cause a predilection for either myotonia (SCM at residue 1306) or the myotonia-paralysis phenotype (PMC at residue 1313).

MATERIALS AND METHODS

Site-directed Mutagenesis

A 5.9-kb cDNA encoding the rat skeletal muscle Na^+ channel α subunit (rSkM1, μl; Trimmer et al., 1989) was subcloned into the EcoRI site of the mammalian expression vector pRC/CMV (Invitrogen, San Diego, CA). A unique silent ClaI site was introduced by a C → T mutation at position 3867 by the method of Deng and Nickoloff (1992) to generate a 503-bp ClaI-SacII mutagenesis cassette. Point mutations corresponding to the human disease mutations G1306A, G1306V, G1306E, and T1313M (residues 1299 and 1306 in rSkM1) were incorporated into the cassette using synthetic oligonucleotides and the PCR overlap extension method (Ho et al., 1989). The fragment was then ligated into the expression construct, and each mutation was verified by sequencing the cassette and flanking regions. The human β_1 subunit cDNA (McClatchey et al., 1993) was subcloned into the EcoRI site of the mammalian expression vector pcDNAI (Invitrogen). Amino acid abbreviations are as follows: G, glycine; A, alanine; V, valine; E, glutamic acid; T, threonine; and M, methionine.

Cell Culture and Transient Transfection

HEK cells were maintained in media containing DMEM with 45 g/liter glucose, 25 mM HEPES, 2 mM L-glutamine, 3 mM taurine, 1% penicillin-streptomycin, and 10% fetal bovine serum. Plasmid DNAs encoding wild-type or mutant rat Na^+ channel α subunits (2.5 μg or 0.3 pmol per 35-mm dish), the human Na^+ channel β_1 subunit (fourfold molar excess over α subunit DNA when used), and a CD8 marker (0.25 μg) were cotransfected into HEK cells by the calcium phosphate method (Sambrook et al., 1989). At 2–4 d after transfection, the HEK cells were trypsinized briefly and passaged to 35-mm dishes for electrophysiological recording. Individual transfection-positive cells were identified with >90% efficiency by affinity for 4.5 μm-diameter microbeads coated with anti-CD8 antibody (Dynal, Inc., Great Neck, NY; Jurman et al., 1994).

Whole-Cell Electrophysiologic Recording

Whole-cell Na^+ currents (1–10 nA) were measured with an Axopatch 200A (Axon Instruments, Inc., Foster City, CA). The amplifier output was filtered at 7 kHz and sampled at 20 kHz using an LM900 interface (Dagan Corp., Minneapolis, MN) controlled by a 486-based computer. Greater than 90% of the series resistance (typically 1–3 MΩ) was compensated by the analog circuitry of the amplifier, and leakage conductance was corrected by digital scaling and subtraction of passive currents elicited by 20-mV depolarizations.

Patch electrodes were fabricated from borosilicate capillary tubes (1.65 mm OD) with a two-stage puller (Sutter Instrument Co., Novato, CA). The shank of the pipette was coated with Sylgard, and the tip was heat polished to a final diameter of 0.5–2.0 μm. The pipette (internal) solution contained (in mM): 130 CsCl, 10 NaCl, 2 $MgCl_2$, 5 EGTA, and 10 Cs-HEPES, pH 7.4. The standard bath contained 140 NaCl, 4 KCl, 2 $CaCl_2$, 1 $MgCl_2$, 5 glucose, and 10 Na-HEPES, pH 7.4. Some cells were placed in the standard bath plus KCl (16 mM total) at the beginning of a recording session. Recordings were made at room temperature (21–23°C) except where indicated otherwise, in which case the temperature was set using a Peltier TC-202 controller (Medical Systems Corp., Greenvale, NY) with bath perfusion at 0.3 ml/min. Tetrodotoxin (TTX) was obtained from Sigma Chemical Co. (St. Louis, MO).

Data Analysis and Kinetic Modeling

Curve fitting was performed manually off-line using AxoBasic and SigmaPlot (Jandel Scientific, San Rafael, CA). Two methods

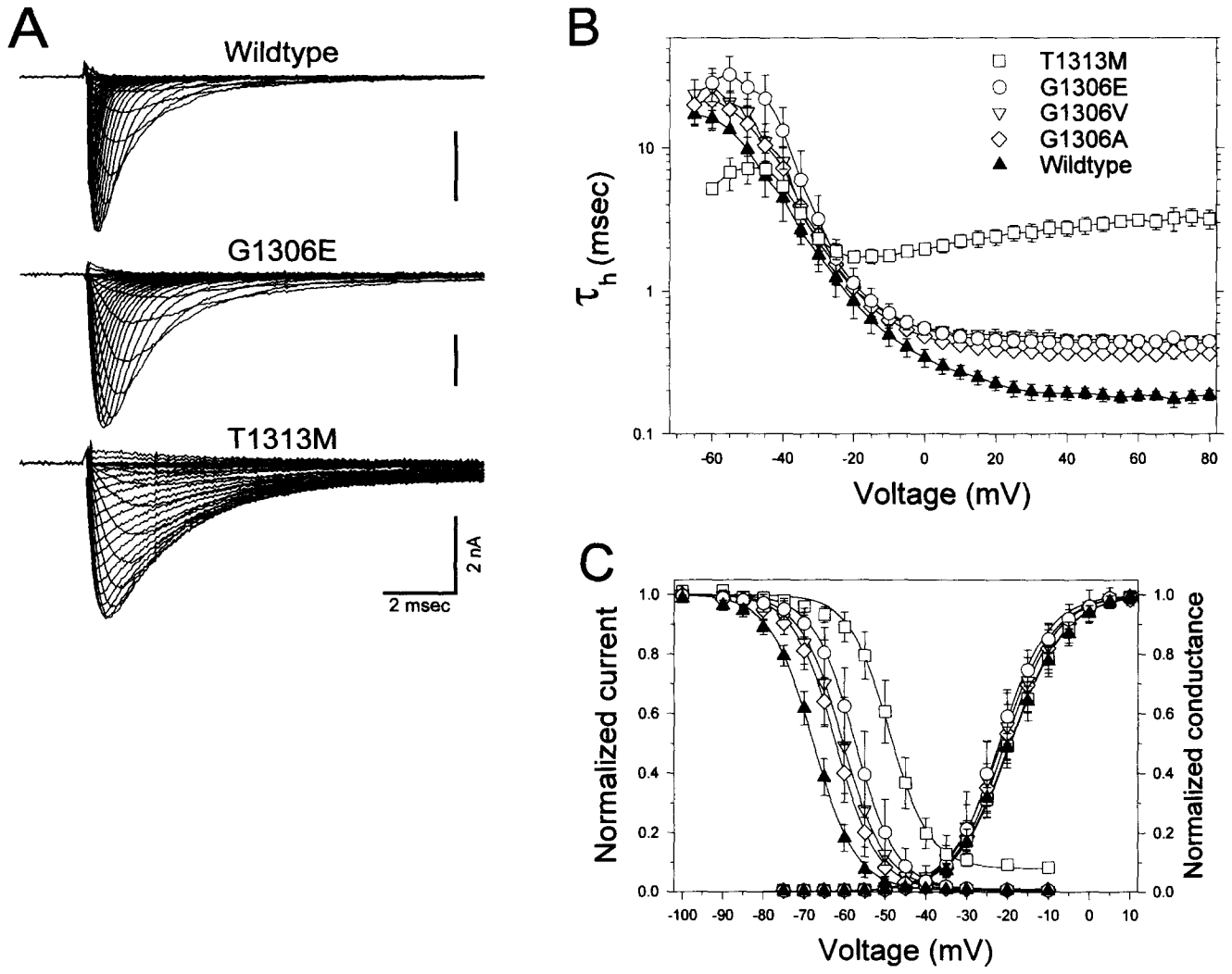

FIGURE 2. III–IV loop mutations alter inactivation of macroscopic Na^+ currents. (*A*) Whole-cell inward currents conducted by Na^+ channels in HEK cells. A family of step depolarizations was made from −120 mV to test potentials over the range of −75 to +80 mV in 5-mV increments. For T1313M, coexpression with the β_1 subunit was necessary to obtain peak currents >1 nA. The α subunit alone was transfected for WT and G1306 mutations. Vertical bars indicate 2 nA for each record. (*B*) Voltage dependence of macroscopic inactivation. τ_h is the dominant (fast) component of a two-exponential fit of the current decay. Note the logarithmic scale for τ_h. (*C*) Voltage dependence of steady-state inactivation, $h_\infty(V)$, in response to a 300-ms prepulse. The nonzero minimum for T1313M reflects the persistent current. $G(V)$ was computed as peak $I_{Na}/(V - E_{rev})$, with E_{rev} obtained from interpolation. Smooth curves were generated using the average values listed in Table I. $V_{hold} = -100$ mV. The bath contained 4 mM [K^+]. Error bars indicate ± SD; n is listed in Table I.

were used to measure the macroscopic inactivation rate, τ_h. For test potentials >-35 mV, the macroscopic decay of the Na^+ current was fitted with a double exponential function, and τ_h was assigned the value of the faster component. The second slower component was always <10% of the total amplitude. For potentials more negative than −30 mV, the depolarization activates very little current, and a two-pulse protocol (Hodgkin and Huxley, 1952) was used to measure the inactivation rate. Conductance was calculated as $G(V) = I_{pk}(V)/(V - E_{rev})$, where the reversal potential E_{rev} was measured experimentally for each cell. Peak I–V relations and steady-state inactivation were fitted well by single Boltzmann functions. Time to half peak was determined by linear interpolation between sampled current points closest to the half-peak value. Except where indicated, all data are presented as mean ± SD.

Nonstationary fluctuation analysis was used to estimate the unitary conductance and the number of channels in a cell so that the open probability could be computed from macroscopic current measurements. For noise analysis, a four-pole Bessel filter was set to 5 kHz, and the sampling rate was 50 kHz. From a run of 256 Na^+ current sweeps, the local mean current $\langle I_{Na} \rangle$ and variance (σ^2) were computed for ensembles of eight sweeps each, and these 32 estimates were then averaged (Sigworth, 1980). Series resistance correction and binning of global $\langle I_{Na} \rangle$ and σ^2 were performed according to Heinemann and Conti (1992). The binned data were fitted by weighted least squares to the relation $\sigma^2 = i_{Na} \times \langle I_{Na} \rangle - \langle I_{Na} \rangle^2/N + c$, where i_{Na} is the single-channel current, N is the number of channels, and c is the background variance.

RESULTS

Myotonia-associated Mutations in the III–IV Loop All Disrupt Inactivation

Macroscopic inactivation rates are slowed. Inactivation was characterized by recording whole-cell Na^+ currents in HEK cells transfected with wild-type (WT) or mutant rat α subunit cDNAs. To minimize the contribution from endogenous Na^+ currents (typically < 50 pA), only cells with peak Na^+ currents >1 nA were included in the kinetic analyses. Conversely, cells with peak currents >10 nA were rejected to minimize series resistance errors. Fig. 2 *A* shows a family of Na^+ current responses to membrane depolarizations from −75 mV to +80 mV in 5-mV increments for representative cells containing WT or mutant Na^+ channels. Mutations at either residue slowed the decay of the macroscopic Na^+ current.

Fig. 2 *B* summarizes the voltage dependence of the fast time constant (τ_h) of decay for WT, G1306A/V/E, and T1313M mutants. The macroscopic decay was most accurately fitted by the sum of two exponential components plus a constant term. Because the faster component accounted for >90% of the current amplitude, macroscopic inactivation of the sodium current was quantified by the fast component only. G1306 mutants inactivated 1.5–2.5-fold more slowly than WT at all voltages. In contrast, the T1313M currents inactivated 20-fold more slowly than WT at potentials more depolarized than 0 mV. Among the mutations at G1306, the rate of inactivation was consistently slower (~twofold) for G1306E at moderately depolarized voltages, −55 to −35 mV.

Both WT and G1306 mutants exhibited a strong voltage dependence of τ_h, with a steep decline between −50 and −10 mV. In contrast, the inactivation rate for T1313M was markedly less voltage dependent at potentials between −30 and +20 mV. A minimum in τ_h occurred at −20 mV and was followed by a gradual increase for larger depolarizations.

For the cells included in Fig. 2, the α subunit alone was transfected for the WT and G1306 mutants. Expression of the T1313M mutant was inefficient using the α subunit alone and typically resulted in 5–10-fold smaller peak Na^+ currents. Since coexpression with the β_1 subunit increases current density in oocytes (Isom et al., 1992), we routinely cotransfected the T1313M α cDNA with a human brain–derived β_1 cDNA (McClatchey et al., 1993) for this study and obtained peak

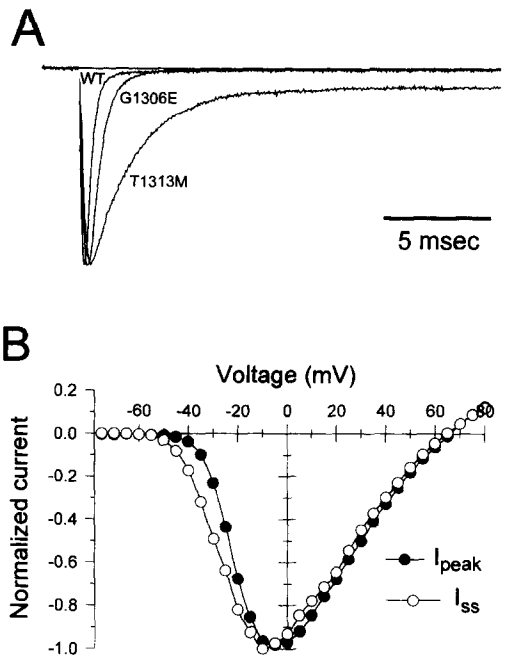

FIGURE 3. The T1313M mutation caused a large noninactivating current. Currents elicited by a step depolarization have been normalized to peak amplitude (5.0 nA for WT, 5.0 nA for G1306E, and 3.9 nA for T1313M) and superimposed. A distinctly larger persistent Na^+ current is conducted by T1313M channels and remained for the duration of the stimulus pulse (50 ms). All cells were cotransfected with the β_1 subunit cDNA. (*B*) Voltage dependence of peak (*solid symbols*) and steady-state (*open symbols*) currents for an HEK cell expressing T1313M channels. Steady-state was defined as the last 5 ms of a 50-ms depolarization. For comparison, the values are normalized to the maximal inward current.

currents within a range comparable to that of WT and G1306 expression. Addition of an exogenous β_1 subunit did not alter the inactivation rate for WT or G1306E currents (compare with Figs. 3 *A* and 8 *A*) and qualitatively did not change the slowed inactivation of T1313M currents.

SCM and PMC mutations shift the voltage dependence of steady-state inactivation. The voltage dependence of steady-state inactivation, $h_\infty(V)$, was determined from the peak current elicited by depolarization to −10 mV, after application of a 300-ms prepulse. Fig. 2 *C* (*left curves*) illustrates $h_\infty(V)$ for WT, G1306A/V/E and T1313M channels. The $V_{1/2}$ of steady-state inactivation was shifted 10.3 ± 2.0 mV (95% confidence interval) in the depolarizing direction for the G1306E mutation, 7.3 ± 2.4 mV for G1306V, and 5.5 ± 1.6 mV for G1306A. The T1313M mutation shifted $h_\infty(V)$ by 17.1 ± 2.1 mV compared with WT. The slope of the Boltzmann fitted to $h_\infty(V)$ was not affected by these mutations (Table I).

T1313M caused a large noninactivating component. Another striking feature that distinguishes the T1313M mutant is the nonzero asymptote for the $h_\infty(V)$ curve at depolarized potentials (Fig. 2 *C*). This plateau occurred because a considerable fraction of the T1313M Na^+ channels (~10% of the number open at the peak) did not inactivate, even after a 300-ms prepulse. The noninactivating component is compared for WT, G1306E, and T1313M in Fig. 3 *A*. Na^+ currents elicited by a depolarization to 0 mV were normalized to peak amplitude and superimposed for cells cotransfected with α (WT, G1306E, or T1313M) and β_1 subunit cDNAs. The G1306E current inactivated about twofold more slowly than WT, as was seen in the absence of exogenous β_1 (Fig. 2 *A*), whereas the T1313M current inactivated sixfold more slowly. These records also demonstrate a large persistent current from the T1313M-transfected cell.

Persistent currents were observed in all experiments, even for WT channels. The persistent current present during the last 5 ms of a 50 ms depolarization is shown for various test potentials for a representative T1313M cell in Fig. 3 *B* (*open circles*, normalized to a maximum of 1.13 nA). Several criteria confirmed that these ionic currents were conducted through Na^+ channels. The reversal potential for the steady-state component was identical to that of the peak I_{Na}, and the voltage dependence paralleled that of the peak I_{Na} (*solid circles*, maximal current 8.2 nA). Moreover, the steady-state current was completely blocked by 5 μM TTX, a specific Na^+ channel blocker. The steady-state component for WT and G1306 mutants, though much smaller, also had a typical Na^+ current-voltage dependence and reversal potential. Secondary leak subtraction of TTX-insensitive currents was used to quantify the amplitude of these small persistent Na^+ currents. The fractional percentage of steady-state to peak Na^+ current at −10 mV, $I_{ss/pk}(-10)$, is listed for each channel type in Table I.

Estimation of open probability by noise analysis. To determine the channel open probability that gives rise to the aberrant persistent current, we used nonstationary fluctuation analysis to estimate the single-channel current, i_{Na}, and number of available channels, *N*. A 20-ms step depolarization from −120 to 0 mV was applied at 0.5-s intervals. Estimates of the mean current $\langle I_{Na} \rangle$ and variance (σ^2) from 256 consecutive trials are shown in Fig. 4 for representative cells containing WT, G1306E, or T1313M channels. Values for i_{Na} and *N* were obtained by least squares (see Materials and Methods), and the open probability was calculated as $P_o = \langle I_{Na} \rangle / (i_{Na} \times N)$. Series resistance effects can cause an overestimation of *N*. The correction proposed by Heinemann and Conti

TABLE I

Parameter Estimates for Na^+ Currents at 22°C

Disease	Mutation	Condition	I_{pk} (nA)	Activation G(v)		$I_{ss/pk}$ (−10 mV)%	Steady-state inactivation h_∞(v)	
				$V_{1/2}$	k		$V_{1/2}$	k
				mV	*mV/e-fold*		*mV*	*mV/e-fold*
Normal	WT	no β_1	5.5 ± 3.1 (9)	−19.2 ± 2.0 (9)	6.74 ± 0.34	0.37 ± 0.13 (9)	−67.7 ± 1.3 (12)	5.36 ± 0.26
		$+\beta_1$	5.7 ± 2.1 (8)	−19.1 ± 4.7 (8)	7.16 ± 0.42	0.40 ± 0.15 (10)	−66.0 ± 2.2 (10)	4.84 ± 0.26
		$\uparrow[K^+] + \beta_1$	4.6 ± 2.5 (7)	−18.6 ± 1.8 (7)	6.99 ± 0.47	0.47 ± 0.23 (8)	−66.7 ± 3.2 (8)	5.07 ± 0.57
SCM	G1306E	no β_1	5.6 ± 2.8 (8)	−22.0 ± 2.5 (8)	5.99 ± 0.38	0.91 ± 0.86 (11)	−57.4 ± 3.2 (16)	5.18 ± 0.65
		$+\beta_1$	6.1 ± 1.5 (7)	−21.1 ± 1.7 (7)	6.08 ± 0.24	0.81 ± 0.42 (14)	−56.3 ± 2.7 (8)	4.99 ± 0.84
		$\uparrow[K^+] + \beta_1$	3.8 ± 1.7 (6)	−21.8 ± 2.3 (6)	6.19 ± 0.40	1.16 ± 0.51 (10)	−58.1 ± 3.0 (9)	4.89 ± 0.43
SCM	G1306V	no β_1	5.0 ± 2.1 (6)	−21.4 ± 3.5 (6)	6.47 ± 0.36	1.44 ± 1.26 (9)	−60.4 ± 3.7 (7)	5.26 ± 0.38
SCM	G1306A	no β_1	3.8 ± 1.5 (7)	−20.5 ± 2.8 (7)	6.35 ± 0.51	0.68 ± 0.24 (10)	−62.2 ± 2.0 (7)	5.20 ± 0.20
PMC	T1313M	$+\beta_1$	4.2 ± 2.2 (8)	−19.4 ± 1.3 (8)	6.76 ± 0.45	11.8 ± 2.8 (15)	−48.9 ± 2.1 (9)	4.98 ± 0.62

Shown are means ± SD (*n*).

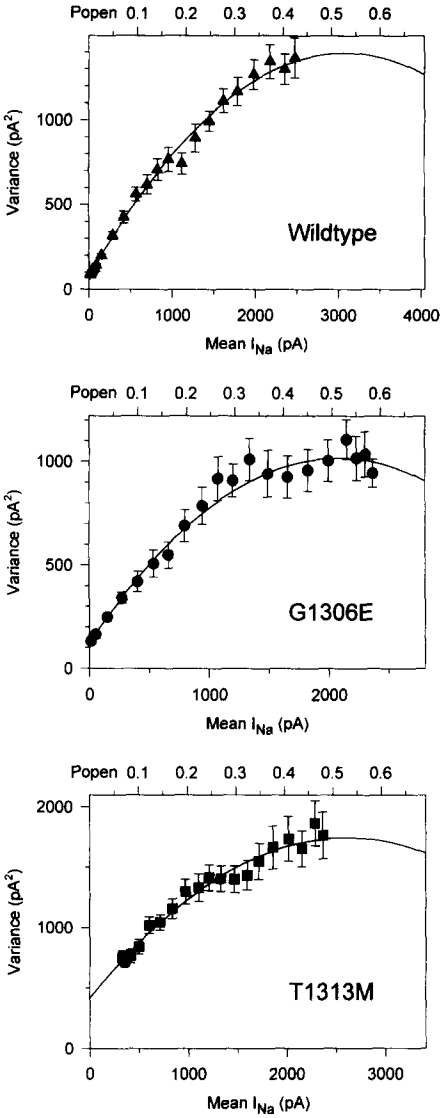

FIGURE 4. The peak open probability was mildly increased for G1306E compared with WT. Mean current ($\langle I_{Na} \rangle$) and variance (σ^2) as measured using non-stationary fluctuation analysis of 256 consecutive trials are shown for representative cells containing WT, G1306E, or T1313M channels. Because of the correction for series resistance, R_s, the peak variance occurs at $P_o = 0.5 *(N\gamma R_s + 1)$, rather than at 0.5 (Heinemann and Conti, 1992). Standard errors are shown. For these cells, i_{Na} = 0.86 (WT), 0.86 (G1306E), and 1.0 (T1313M) pA/channel and N = 6810 (WT), 4710 (G1306E), and 4832 (T1313M) channels. V_{hold} = −100; V_{pre} = −120; repetition interval = 0.5 s; Bessel filter = 5 kHz.

(1992) was applied, which reduced the estimate of N by ~3% [$N/N_{meas} = 1/(N_{meas}\gamma R_s + 1) \approx 1/(2{,}000 \times 15 \times 10^{-12} \times 10^6 + 1) = 0.97$]. The peak P_o was consistently higher for G1306 mutants than for WT channels, but was unchanged for T1313M (Table II). In contrast, the steady-state P_o was an order of magnitude larger for T1313M compared with the 1306 mutants or WT channels.

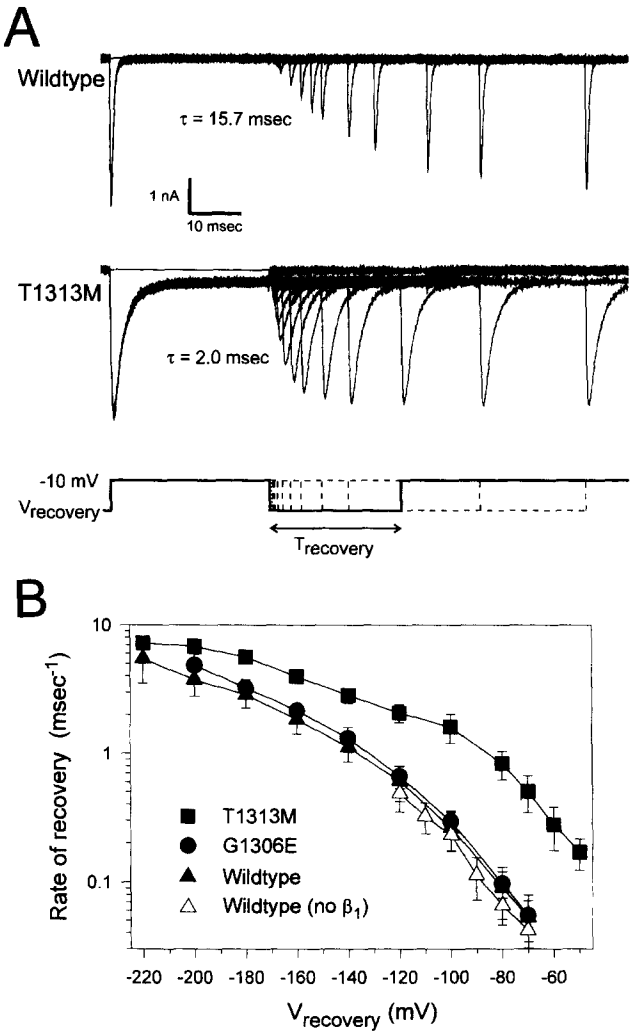

FIGURE 5. Recovery from inactivation was faster for T1313M compared with WT or G1306E. Traces in *A* show superimposed trials for a recovery voltage of −80 mV. Between trials, the membrane potential was held at −100 mV for 500 ms. The fractional recovery was best fitted by the sum of two exponentials (τ_{fast} and τ_{slow}); the amplitude of the minor τ_{slow} component (not shown) was always <20% of the total. (*B*) The voltage dependence of the fast recovery rate, computed as $1/\tau_{fast}$, is shown as mean ± SD for n = four–nine cells.

T1313M hastens recovery from inactivation. Recovery from inactivation was measured using a two-pulse protocol (Fig. 5 *A*) for WT, G1306E, or T1313M channels. After an initial depolarizing pulse of −10 mV for 30 ms to fully inactivate channels, the cell was held at the recovery voltage for a variable time (0.05–60 ms) and a second pulse to −10 mV was applied to measure the fractional recovery. Recovery was best fitted by the sum of two exponential components. A fast component (τ_{fast}) predominated, accounting for >80% of the current amplitude. The remaining component of recovery from inactivation had an ~10-fold slower time con-

TABLE II

Estimates of Open Probability at 0 mV from Noise Analysis

	WT	G1306A	G1306V	G1306E	T1313M
Peak P_0	0.48 ± 0.04 (6)	0.59 ± 0.08 (5)	0.62 ± 0.11 (5)	0.60 ± 0.07 (4)	0.51 ± 0.05 (4)
Steady-state P_0	0.0019	0.0040	0.0087	0.0049	0.061
i_{Na} (pA)	0.86 ± 0.06	0.96 ± 0.11	0.98 ± 0.07	0.90 ± 0.09	0.91 ± 0.08
γ (pS)	13 ± 0.9	14 ± 1.6	15 ± 1.1	13 ± 1.3	14 ± 1.2

Shown are means ± SD (n). $P_0 = \langle I_{Na} \rangle / (i_{Na} \times N)$ where the unitary current, i_{Na}, and number of channels, N, were estimated from the noise analysis and $\langle I_{Na} \rangle$ is the ensemble average of the whole-cell current. Steady-state P_0 was calculated as peak $P_0 \times (I_{ss}/I_{pk})$ from Table I.

stant. The voltage dependence of the fast recovery rate ($1/\tau_{fast}$) shown in Fig. 5 *B* indicates that the T1313M channel recovered three- to sevenfold faster than WT over the voltage range −120 to −70 mV. At hyperpolarized potentials, recovery approached a maximum rate comparable to WT. Recovery of the G1306E mutant did not differ significantly from that of WT. The coexpression of exogenous β_1 subunits also had no significant effect on the WT channel recovery rate (Fig. 5 *B*).

Tail Currents Are Slowed for G1306E and T1313M Channels

Tail currents were recorded from WT, G1306E, and T1313M cells to compare rates of deactivation. As shown in Fig. 6 *A*, a brief (0.4-ms) step to +40 mV rapidly opened channels, and subsequent repolarization caused a rapid voltage-dependent decay of the Na^+ current. Beyond the 80-μs transient caused by nonlinear components remaining after leak subtraction (Fig. 6 *A*, *open symbols*), the decline in Na^+ current was fitted well by a single exponential, τ_{tail}. Fig. 6 *B* summarizes the voltage dependence of τ_{tail} over a −60 to −100-mV range. The tail decay was fastest for WT channels and was slowed ~1.3-fold for G1306E and 1.7-fold for T1313M mutants. The decline in Na^+ current during tails reflects the decay in open state occupancy, which might involve deactivation (O → C), inactivation (O → I), or even reopening (C → O). Reopening is unlikely at potentials of −60 mV or less, as shown by Fig. 2 *C*. Differences in microscopic inactivation rate constants

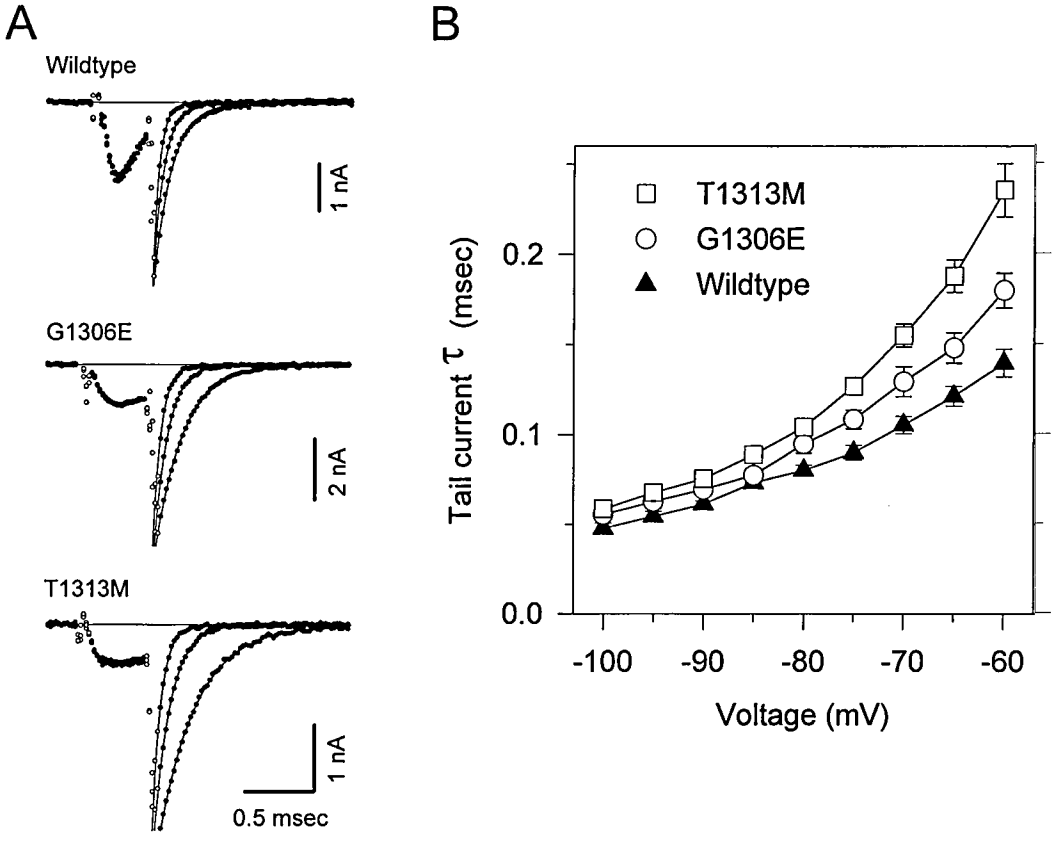

FIGURE 6. Tail currents decayed slower for the mutants compared with WT. Representative tail currents in *A* were elicited by a 0.4-ms (WT) or 0.5-ms (G1306E, T1313M) voltage step to +40 mV followed by repolarization to potentials between −60 and −100 mV. After the residual capacitance transient (*open circles*), the current was fitted by a single exponential decay (*lines*). Currents were filtered at 10 kHz (four-pole Bessel) and sampled every 20 μs. (*B*) The voltage dependence of the tail current time constant (τ_{tail}) is shown as mean ± SEM for n = four–six cells.

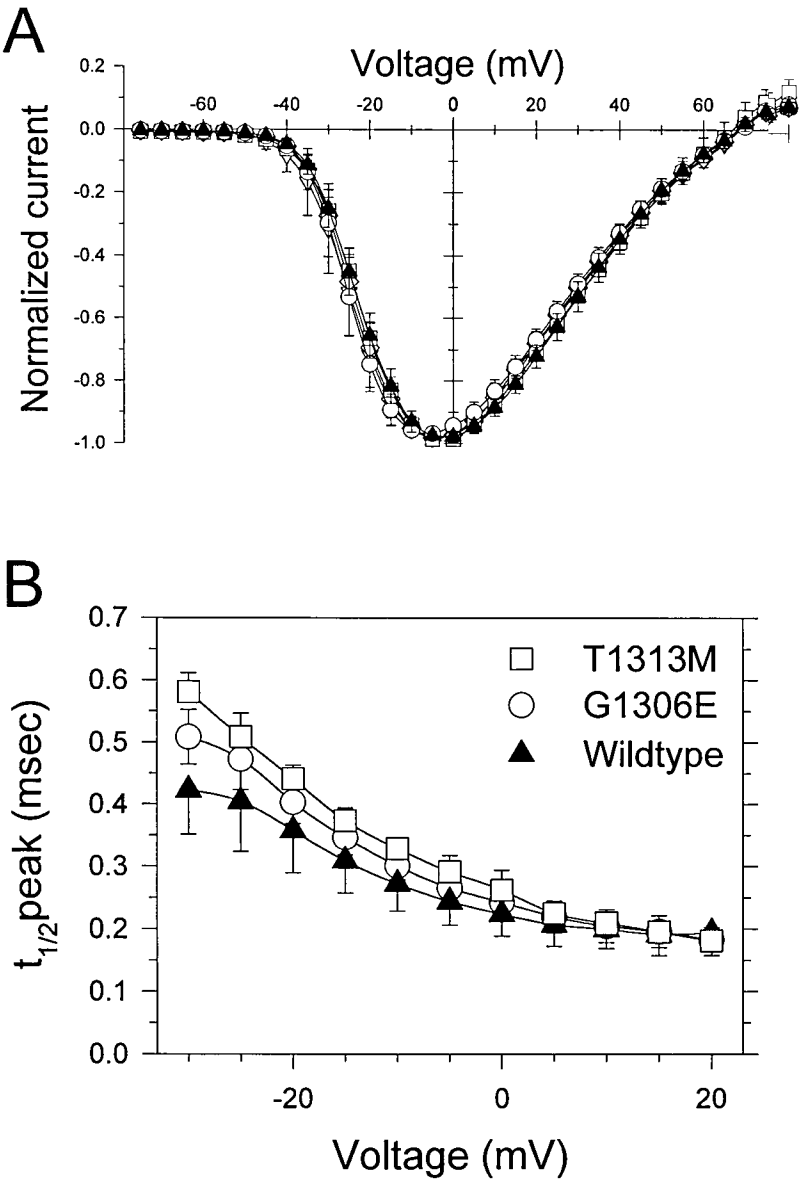

FIGURE 7. Activation properties of WT and mutant channels. (*A*) Peak Na^+ current elicited at varying test potentials was normalized to the maximum current for each cell. The voltage dependence and reversal potential were comparable between WT and all mutants. *n* is listed in Table I. (*B*) Time to half-peak is only mildly prolonged for mutant channels. Values are mean ± SD, *n* = eight–nine cells, not corrected for the delay introduced by the Bessel filter (84 μs).

(Fig. 2 *B*), however, may contribute significantly to the divergence of τ_{tail} in Fig. 6 *B*, especially at potentials more depolarized than −80 mV. The convergence of the data over the −85 to −100-mV range in Fig. 6 *B* and estimates of rate constants for transitions near the open state (see Discussion) both imply that the transition rate for deactivation from the open to its preceding closed state was not greatly altered by the G1306E or T1313M mutation.

Mutations Do Not Alter Activation or Permeation

The voltage dependence of the peak Na^+ current provides a measure of channel activation and selectivity. Fig. 7 *A* shows the normalized peak Na^+ current for WT and mutant channels. In contrast to the dramatic effects upon measures of inactivation, none of the mutations altered the peak current–voltage relation. Fig. 2 *C* (*right curves*) shows relative conductance $G(V)$ for WT, G1306A/V/E, and T1313M+β_1 mutant Na^+ channels. The half-maximal voltage ($V_{1/2}$) and the slope of the Boltzmann-fitted $G(V)$ curves were similar for WT and each mutant (Fig. 8 *B*, Table I). Coexpression of the β_1 subunit also had no significant effect on these parameters (Table I).

Another measure of activation is the time to half-peak of the Na^+ current. Since the peak is determined by competition between activation and inactivation, which have comparable rates, a change in either could affect this measurement. Fig. 3 *A* shows that the peak occurred slightly later for mutant channels compared with WT. This difference is quantified as time to half-peak for G1306E and T1313M channels compared with

WT in Fig. 7 *B*. Time to half-peak was slowed by 15% for G1306E and 25% for T1313M at −20 mV. In view of the prediction that slowed inactivation (shown to exist for these mutants) is expected to delay the time to peak, the mild changes shown in Fig. 7 *B* imply that activation was not substantially altered, compared with the large changes for inactivation (τ_h, $V_{1/2}$, and I_{ss}).

Two independent measures showed that ion permeation was not affected by the mutations. The reversal potentials were unchanged (Fig. 7 *A*), which implies that mutant channels select for Na^+ over other cations, as do WT channels. Also, as seen in Table II, the single-channel conductance was not affected by the mutations.

Increased $[K^+]_o$ Mildly Exacerbates the Inactivation Defects in G1306E

Myotonia is worsened by K^+ loading in patients with SCM mutations (Ricker et al., 1994), but not T1313M (Jackson et al., 1994). To determine if the SCM-associated inactivation defects in HEK cells are similarly K^+ sensitive, Na^+ currents were recorded from cells bathed in either 4 or 16 mM $[K^+]_o$. Although 16 mM $[K^+]_o$ is higher than the serum $[K^+]$ in affected patients, it is comparable to the T-tubular and local tissue $[K^+]_o$ after a train of action potentials (Freygang et al., 1964). A fourfold elevation of $[K^+]_o$ caused a mild slowing of τ_h by 10–20%, for both WT and G1306E mutants coexpressed with a β_1 subunit (Fig. 8 *A*). The voltage dependence of steady-state inactivation was not affected, as shown in Fig. 8 *B* and Table I. In contrast, elevated $[K^+]_o$ had a differential effect on the persistent current of G1306E compared with WT (Fig. 8 *C*). In normal $[K^+]_o$, the fraction of noninactivating current was greater for G1306E than WT. Elevated $[K^+]_o$, however, caused a further increase in the noninactivating Na^+ current in G1306E ($P < 0.05$, rank sum test), whereas the behavior of WT channels remained unchanged.

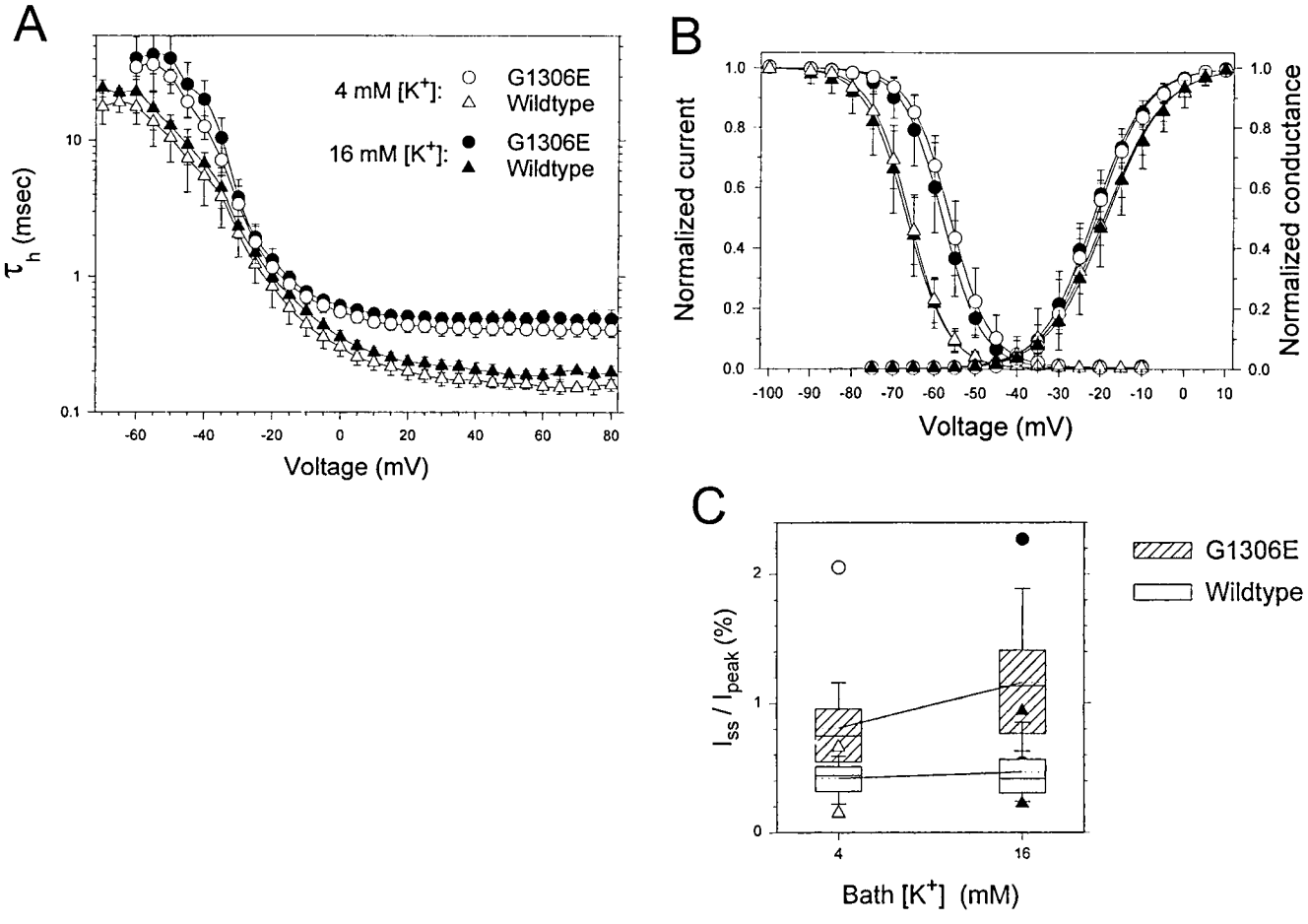

FIGURE 8. Elevated $[K^+]_o$ caused only small changes in Na^+ channel behavior. (*A*) Macroscopic current decay (τ_h) was mildly slowed in 16 mM $[K^+]_o$ for both WT and G1306E channels; *n* is listed in Table I. (*B*) Elevated $[K^+]_o$ did not alter steady-state inactivation or the voltage dependence of peak conductance. Curves were computed using the average values in Table I. (*C*) Elevated $[K^+]_o$ mildly increased the noninactivating component of I_{Na} for G1306E but not WT channels. Boxes indicate 25th to 75th percentiles; bars represent 10th and 90th percentiles; dotted lines show mean values; symbols plot extreme values; n = 10 cells for WT and 14 cells for G1306E.

Temperature Sensitivity of Na^+ Current Inactivation

The temperature sensitivity of inactivation was evaluated for WT, G1306E, and T1313M channels over 8–37°C. Fig. 9 *A* shows representative whole-cell currents for each channel at 12, 17, 22, 27, and 33°C. The inactivation time constant (τ_h) was clearly faster at higher temperatures for mutant and WT channels. The temperature sensitivity of τ_h at 0 mV is shown as an Arrhenius plot in Fig. 9 *B*. The regression slopes were comparable for WT and T1313M, but consistently smaller for G1306E channels and correspond to Q_{10} values (fold change between 17 and 27°C) of 3.34 ± 0.09, 3.45 ± 0.20, and 2.81 ± 0.06, respectively. Thus, at 0 mV, there was no detectable difference in the temperature sensitivity of τ_h for WT and T1313M, a mutant associated with cold-aggravated myotonia. To determine whether a difference in temperature sensitivity may occur at other potentials, the Q_{10} for macroscopic current decay was measured over a range of voltages. Fig. 9 *C* shows that the Q_{10} of $\tau_h(V)$ was comparable for WT and T1313M over a 70 mV range and that G1306E was consistently less temperature sensitive.

The amplitude of the persistent Na^+ current, mea-

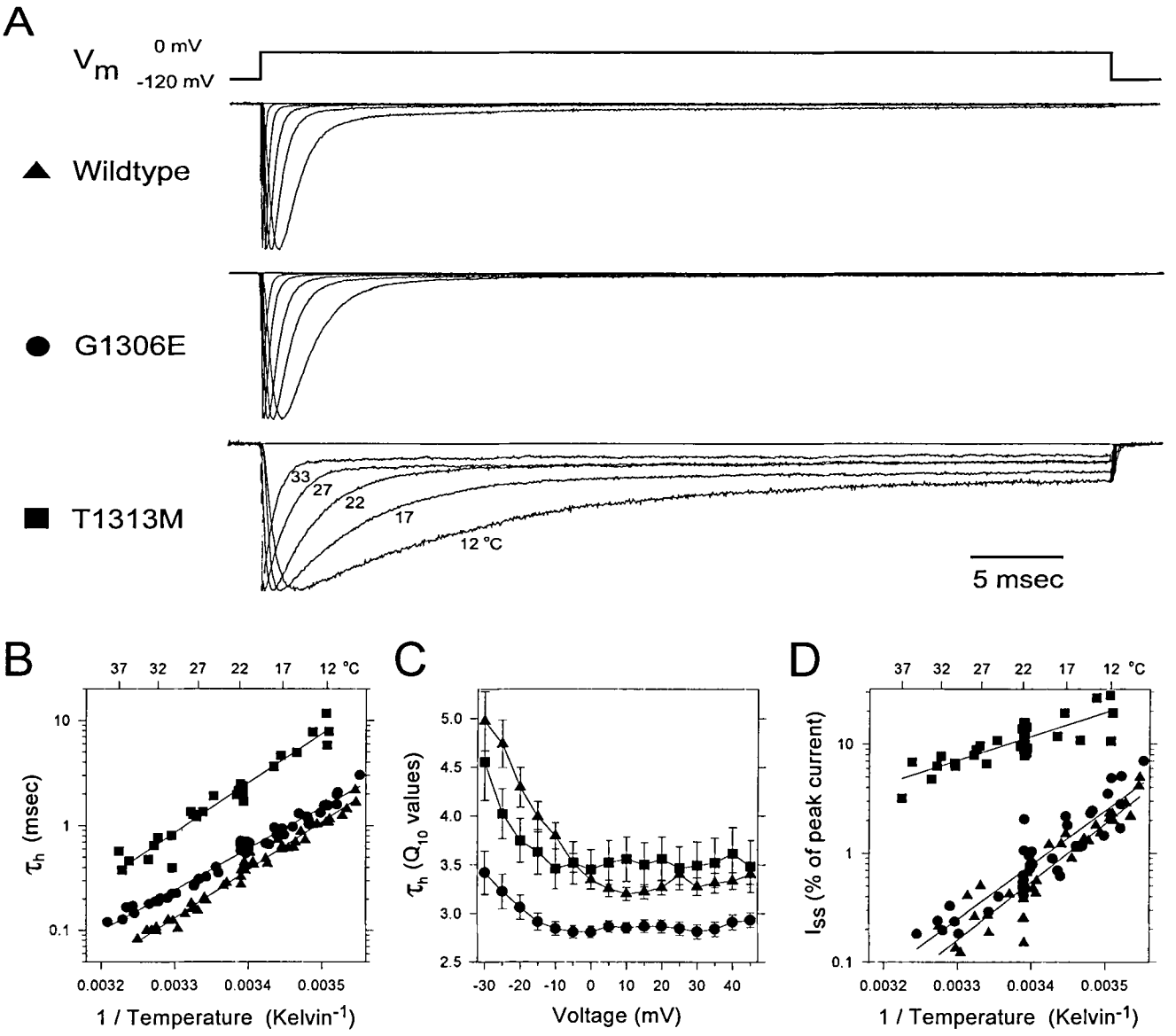

FIGURE 9. The temperature sensitivity of inactivation was similar for WT and mutant Na^+ channels. (*A*) Normalized currents are shown for WT, G1306E, or T1313M channels at several temperatures. (*B*) Arrhenius plot of τ_h at $V = 0$ mV for each type of channel. (*C*) The $Q_{10}(V)$ for τ_h remained comparable for WT, G1306E, and was smaller for T1313M channels over the entire 70-mV range. Temperature sensitivity increased at modest depolarization (−30 to −10 mV). (*D*) Arrhenius plot shows that the amplitude of the steady-state current at the end of a 50-ms depolarization to −10 mV was less temperature sensitive for T1313M than for WT or G1306E.

sured as a fraction of the initial peak, was also modified by changes in temperature. Cooling caused an increase in the normalized steady-state current for WT and both mutants (Figure 9 *A*). An Arrhenius plot of the persistent current at −10 mV (Fig. 9 *D*) shows that, although the amplitude of noninactivating component was much larger for T1313M than WT or G1306E, the temperature sensitivity was actually smaller (Q_{10} 1.79 ± 0.13 for T1313M, 4.02 ± 0.35 for WT, and 3.74 ± 0.37 for G1306E).

DISCUSSION

All Myotonia-associated Mutations in the III–IV Linker Disrupt Inactivation

The primary functional defect in all four of the myotonia-associated mutations of the Na^+ channel III–IV linker is a disruption of inactivation. A selective effect on inactivation was expected from these mutations, based on previous mutagenesis and site-directed antibody experiments in this region (reviewed in Catterall, 1992). The results from our study further define critical residues of the III–IV linker, but more importantly, they provide a quantitative comparison of functional defects caused by four disease mutations that have distinct phenotypes. The inactivation defects caused by the mutation at T1313 differed significantly from those caused by substitutions at G1306, and these differences almost certainly contribute to the distinct phenotypes of myotonia plus paralysis (PMC) versus myotonia alone (SCM).

The SCM mutations at G1306, when tested in rSkM1 expressed in HEK cells, slowed macroscopic inactivation (τ_h) about twofold, shifted steady-state inactivation by 5–10 mV in the depolarizing direction, and increased the steady-state current two- to threefold. Similar results were observed for Na^+ currents in sarcolemmal blebs of muscle from patients (Lerche et al., 1993) or in HEK cells transfected with cDNA coding for human SkM1 with the G1306A, V, or E mutation (Mitrovic et al., 1995). This consistency supports the premise that Na^+ channels heterologously expressed in HEK cells have functional properties comparable to endogenous SkM1 expressed in muscle, and that the rat and human isoforms of SkM1 behave similarly.

The PMC mutation in rSkM1 corresponding to T1313M in hSkM1 caused a much greater change of inactivation. In HEK cells, this Na^+ channel exhibited a 20-fold slower τ_h at depolarized potentials, with diminished voltage dependence of τ_h at potentials between −30 and +20 mV. For T1313M only, a minimum in τ_h occurred at moderate depolarizations, near −20 mV (Fig. 2 *B*). O'Leary and colleagues (1995) observed a similar phenomenon for another mutation in the III–IV loop, Y1494Y1495 to QQ in the cardiac α subunit (hH1), which also causes a marked slowing of τ_h. We agree with O'Leary et al. (1995) that the gradual increase in τ_h at depolarized potentials for these mutants most likely originates from the voltage dependence of deactivation. Normally, the voltage dependence of τ_h is dominated by the coupling of voltage-insensitive microscopic inactivation to highly voltage-dependent activation (Aldrich and Stevens, 1987). At potentials >0 mV, the transitions to opening are fast compared with the inactivation rate, which in turn is much faster than the deactivation rate. Consequently, channels tend to open only once, and τ_h approaches the mean open time, which is approximately constant and equal to the reciprocal of the microscopic inactivation rate. If a mutation lowers the open to inactive transition rate, then deactivation and inactivation rates are comparable over the 0–40 mV range. Because of the influence of deactivation, the mean open time continues to increase over an extended range of depolarized potentials. The extended range for the voltage dependence of the mean open time causes τ_h to increase with depolarization. This effect was confirmed using the model for Na^+ channel gating proposed by Kuo and Bean (1994), with the O → I rate reduced by 20-fold to simulate T1313M. This change not only causes τ_h to approach 3 ms at +80 mV, but also produces a minimum near −20 mV.

The steady-state inactivation curve, $h_\infty(V)$, was markedly shifted to the right (depolarized) for T1313M. This 17-mV shift cannot be produced solely by a 20-fold reduction in the rate of the O → I transition discussed above. We have performed simulations with the Kuo and Bean model (1994) to show that a reduction in the rate of inactivation from closed states (C → I) causes a large depolarizing shift in $h_\infty(V)$. This analysis supports the notion that the T1313M mutation in the III–IV linker shifts the equilibrium between closed and inactive states, in addition to the altered transitions between open and inactive states described below. Furthermore, the $h_\infty(V)$ curve approached a nonzero minimum for T1313M (~ 10% of the initial peak) at strongly depolarized voltages. Failure of T1313M channels to fully inactivate was also observed directly in currents elicited by depolarizing voltage steps (Fig. 2 *A*). Persistent Na currents occurred at all potentials >−40 mV (Fig. 3 *B*), which implies there must be a nonzero pedestal to $h_\infty(V)$, and not merely a shift in the midpoint. Tahmoush et al. (1994) also observed an abnormal persistent Na^+ current (~5% of peak) in ensembled data from cell-attached patch recordings on muscle cultured from a patient with the T1313M mutation. When Yang and colleagues (1994) expressed T1313M in the human isoform of SkM1, τ_h was dramatically slowed, but $h_\infty(V)$ was shifted by only 9 mV, and the steady-state current was smaller than we observed in the rat isoform of SkM1. Although no functional differences have pre-

viously been identified between rSkM1 and hSkM1, this discrepancy may arise from a species difference. Rat SkM1 and hSkM1 differ within the III–IV linker only by a Phe to Leu at 1305, but the as-yet uncharacterized receptor for the inactivation particle could be less well conserved. Alternatively, the difference may be attributable to the use of fluoride in the patch pipette (Yang et al., 1994), which may chelate divalents and alter the state of phosphorylation.

Kinetic Model of the Gating Changes

A reduced kinetic model of Na^+ channel gating can be used to summarize and compare the effects of the various III–IV linker mutations in terms of transition rates or energy differences between specific states. This simplified model assumes a single open state, and hence is not sufficient to produce shifts between normal and noninactivating modes of gating observed for some (Cannon et al., 1991; Cannon et al., 1993; Cannon et al., 1995), but not all Na^+ channel mutants (Chahine et al., 1994). Our whole-cell data provide information primarily limited to transition rates into and from the open state, and the analysis is limited to the reduced scheme below:

$$C \underset{k_{OC}}{\rightleftharpoons} O \underset{k_{off}}{\overset{k_{on}}{\rightleftharpoons}} I.$$

At strongly depolarized potentials, activation through closed states is rapid, the deactivation rate is negligibly small, and the macroscopic decay of the Na^+ current is primarily determined by transitions between the open and inactive states (Aldrich and Stevens, 1987). Under these conditions, the on rate of the inactivation particle is $k_{on} = (1 - P_o ss)/\tau_R$, where $P_o ss$ is the steady-state open probability, and $\tau_R = 1/(k_{on} + k_{off})$ is a relaxation time numerically equal to the limiting value of τ_h at potentials >40 mV. Because $P_o ss$ is small compared to one, the estimate of k_{on} depends primarily on the asymptotic value of τ_h at depolarized potentials. Conversely, $P_o ss$ and τ_h both strongly influence the estimate of the unbinding rate, $k_{off} = P_o ss/\tau_R$. Because neither I_{ss}/I_{pk} (Fig. 3 *B*) nor τ_h (Fig. 2 *B*) vary significantly over a 60-mV range (+20 to +80), we have assumed that k_{off} is voltage independent. The steady-state open probability at strongly depolarized potentials (>60 mV) was computed from the ratio $I_{ss/pk}$ and the value of the peak P_o at 0 mV from the fluctuation analysis. The ratio of I_{ss} to I_{pk} was constant at voltages ≥ -10 mV (Fig. 3 *B*) and is listed in Table I. The fluctuation analysis could not be used to estimate $P_o ss$ at voltages >10 mV because the lower driving force for Na^+, faster current decay, and larger capacitance transients all reduced the accuracy of the measurements. To estimate $P_o ss$ at depolarized voltages, the value of the peak P_o at 0 mV was scaled by the peak permeability, $\Gamma(V)$, as estimated from the GHK current equation:

$$P_o ss(V \to \infty) = (I_{ss}/I_{pk}) \times P_o(0\text{ mV}) \times \Gamma(V \to \infty)/\Gamma(0\text{ mV}).$$

For WT and mutant channels, $\Gamma(V)$ had nearly achieved its maximal value by 0 mV so that the scale factor, $\Gamma(V \to \infty)/\Gamma(0\text{ mV})$, was ~1.25. The rate constants estimated by this technique are listed in Table III. The altered inactivation kinetics are primarily caused by a reduction in the on rate of the inactivation gate, about twofold for G1306 mutants and 20-fold for the T1313 mutation. Conversely, the off rate of the inactivation gate was either unchanged (G1306A, G1306E) or only mildly hastened by 1.7-fold (G1306V, T1313M). The model predicts a dramatic increase, ~20-fold, in the mean open time at strongly depolarized potentials for T1313M. A much smaller increase was observed by Tahmoush et al. (1994) because unitary Na^+ currents were measured at −40 mV, where the large increase in deactivation rate limits the open time and causes increased bursts of reopenings. The energetic "cost" of the T1313M mutation is a destabilization of the inactive state by 2.0 kcal/mol as revealed by the change in free energy, ΔG (Table III). This energy difference is equivalent to 3.4RT at room temperature or a 30-fold increase in the dissociation constant, k_{off}/k_{on}.

The deactivation rate from the open state, k_{oc}, can be estimated from the tail current data (Fig. 6). In the absence of reopenings, that is, at potentials <−50 mV from Fig. 2 *C*, the reciprocal of τ_{tail} equals the sum of the rates for leaving the open state, $k_{on} + k_{oc}$. The microscopic inactivation rate, k_{on}, was estimated from $P_o ss$ and τ_h as the membrane potential approached +80 mV. Depolarization to +200 mV (data not shown) did not cause any further change in τ_h and demonstrates that k_{on} has little, if any, voltage dependence, as has been observed by others (Aldrich and Stevens, 1987; Cota and Armstrong, 1989). Consequently, it is reasonable to assume that over the range of our tail current measurements, −60 to −100 mV, k_{on} is approximately the value determined at +80 mV (Table III). The deactivation rate, $k_{oc}(V)$, was estimated as $[1/\tau_{tail}(V)] - k_{on}$. Similar strategies for dissecting k_{on} and k_{oc} from tail current measurements have been used by Cota and Armstrong (1989). Fig. 10 shows the effect of subtracting k_{on} in the calculation of $k_{oc}(V)$. The data from Fig. 6 *B* are redrawn as the reciprocal of τ_{tail} for each channel type (*solid symbols*). Open symbols show the shift in these data produced by subtracting k_{on}. The correction for k_{on} effects was greatest for WT and least for T1313M channels and reduces the difference in the estimate of k_{oc} between channel types. Parameter values for monoexponential fits of the shifted data are listed as k_{oc} in Table III. We conclude that the G1306 and T1313 mu-

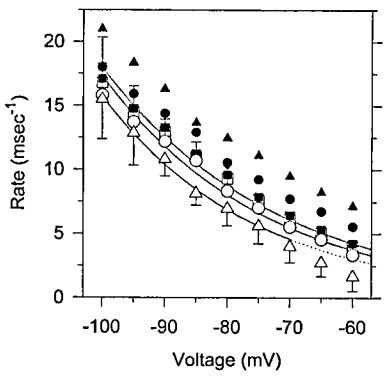

FIGURE 10. Estimate of deactivation rates. Data from Fig. 6 *B* are redrawn as reciprocal τ_{tail} (*solid symbols*). The deactivation rate was computed as $1/\tau_{tail} - k_{on}$ from Table III and is shown by open symbols; error bars show SD. Exponential fits of the shifted data (*open symbols*) yielded deactivation rates (s^{-1}) at 0 mV and voltage sensitivities (mV/e-fold) of 260 and 24.3 for WT (*triangles*), 370 and 26.0 for G1306E (*circles*), and 490 and 27.7 for T1313M (*squares*). For WT only, the fit was limited to data where $V \leq -70$ mV; dashed line shows an extrapolation to more positive voltages.

TABLE III

Rate Constants for the Reduced Model

Mutant	k_{oc}	k_{on}	k_{off}	$\Delta G_{on/off}$
WT	$260\ e^{-V/24}$	5,500	14	−3.5
G1306A	—	2,700	14	−3.1
G1306V	—	2,200	24	−2.7
G1306E	$370e^{-V/26}$	2,200	13	−3.0
T1313M	$490e^{-V/28}$	290	24	−1.5

Rates are in s^{-1}, voltages in mV, and changes in free energy in kcal/mol. Free energy was computed as $\Delta G = -RT \ln(k_{on}/k_{off}) = -RT \ln(1/P_{0ss} - 1)$.

tations in the III–IV loop do not markedly alter the deactivation rate. The apparent difference in deactivation rate seen in the raw tail currents (Fig. 6) occurs because of the effect of differences in microscopic inactivation rates over the −60 to −85 mV range. Mitrovic et al. (1995) reported that deactivation is moderately slower (approximately twofold) for G1306 mutants than WT. Although their data for moderately hyperpolarized tail potentials (−65 to −100 mV, at 22°C) were not corrected for k_{on}, more hyperpolarized measurements to −160 mV at 10°C, where k_{on} effects should be negligible, also showed a slower τ_{tail} for mutants.

The disruption of inactivation caused by mutations at G1306 and T1313 is consistent with proposed structural mechanisms in which the III–IV loop acts as a "ball" (Armstrong and Bezanilla, 1977) or "hinged lid" (West et al., 1992) that occludes the inner mouth of the ion conduction pathway. West and colleagues (1992) showed that a triplet of hydrophobic residues in the III–IV linker, IFM, is a critical component of the fast inactivation mechanism. T1313 is the next residue downstream from the IFM, and substitution for threonine by a bulkier methionine could sterically hinder the binding interaction. The T1313M mutation destabilizes the inactive state to a greater extent than those at G1306 as reflected in the larger reduction of $\Delta G_{on/off}$ by 2.0 vs 0.4–0.8 kcal/mol, respectively (Table III). Destabilization of the inactive state may also contribute to the hastened recovery from inactivation seen for T1313M (Fig. 5), although our reduced kinetic scheme cannot be used to model these transitions. West and colleagues (1992) have proposed that the pair of glycines at positions 1306–1307 may form a hinge point in the III–IV loop. One prediction from such a model is that substitution by residues with larger side chains would reduce the flexibility of the hinge. Each mutation at G1306 reduced the on rate, k_{on}, for the inactivation gate (Table III), which is consistent with the structural model. Mutations at G1306 also shift the equilibrium toward the open state (reduced $\Delta G_{on/off}$ compared with WT in Table III) as demonstrated by the increase in steady-state P_o.

Functional Consequences of the Inactivation Defects: A Predilection for Myotonia or Myotonia Plus Paralysis

The kinetic measurements from the preceding experiments were incorporated into our mathematical model of a muscle cell (Cannon et al., 1993) to determine whether the observed abnormalities, and in particular differences between specific mutations, could account for associated clinical phenotypes. The model consists of two electrically coupled membrane compartments to simulate the sarcolemma and T-tubules. Both compartments contain voltage-gated Na^+ and K^+ channels simulated by the Hodgkin-Huxley equations and a leakage conductance. Finally, the $[K^+]$ of the T-tubule changes because of a balance between increases from activity-driven egress of intracellular K^+ and decreases by passive diffusion. Changes in T-tubular $[K^+]$ influence the excitability of the system by altering the reversal potential for the K^+ and leakage conductances in the T-tubule compartment. The inactivation parameter, $h(V,t)$, was modified for a portion of the total pool of Na^+ channels to simulate the changes in $\tau_h(V)$, $h_\infty(V)$, and steady-state P_o for the heterozygous state with WT and G1306E or WT and T1313M mutations (see Appendix).

Fig. 11 *A* depicts a simulated response to injection of a 150-ms current pulse, using baseline WT parameters. In this state of normal excitability, a single action potential is elicited, and the membrane repolarizes at the end of the stimulus. To simulate the G1306E mutation, $\tau_h(V)$ was modified to match the data in Fig. 2 *B*, a small noninactivating component to I_{Na} was added ($I_{ss}/I_{pk} = 0.008$), and a 10-mV depolarizing shift was incorporated in the $h_\infty(V)$ curve. The same current pulse elicited a train of repetitive discharges during the stimulus (Fig. 11 *B*). If the initial extracellular $[K^+]$ is increased from 4 to 5 mM, then after-discharges persist beyond the stimulus. After-discharges produce the stiffness or delayed relaxation of tension after voluntary contraction in myotonic muscle. The pattern of after-

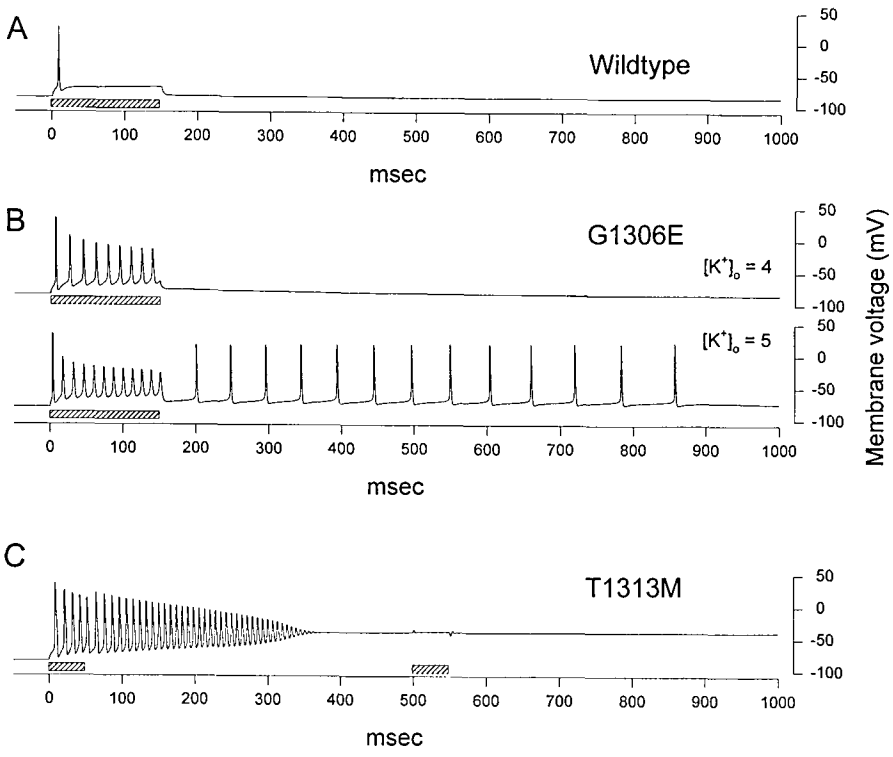

FIGURE 11. Simulated responses to injected current pulses predicts myotonic behavior for cells containing G1306E channels and myotonia plus depolarization block for those with T1313M. (*A*) WT response, using baseline parameters from Cannon et al. (1993) elicits a single action potential. (*B*) Simulations incorporating the inactivation defects for G1306E generates repetitive firing (myotonia) after the same stimulus. (*C*) When the Na^+ conductance simulates T1313M defects, in particular the large noninactivating component, a brief stimulus elicits early repetitive, widened action potentials and later decreased excitability from sustained depolarization of the membrane. A 25-$\mu A/cm^2$ stimulus current was applied during the interval indicated by the shaded bars.

discharges in Fig. 11 *B* is comparable to the appearance of myotonia in clinical electromyograms. These examples illustrate how the consequence of a fixed Na^+ channel defect can vary with basal $[K^+]_o$. Two mechanisms contribute to the repetitive firing. The defects in Na^+ channel inactivation enhance the excitability such that multiple discharges are elicited during the stimulus. Secondly, T-tubular K^+ accumulation provides the depolarizing influence that generates the after-discharges.

The simulated response for a muscle containing Na^+ channels with the T1313M mutation is shown in Fig. 11 *C*. Sodium channel gating has been modified to reproduce the 20-fold slowing and altered voltage dependence of τ_h, the large persistent Na^+ current (I_{ss}/I_{pk} = 0.12), and the 19-mV depolarized shift of steady-state inactivation. The combination of pronounced slowing of inactivation and a large persistent current produces an increase in the action potential duration because repolarization is dependent upon inactivation of the Na^+ current. Potassium efflux into the T-tubule is greatly augmented by the longer duration of the depolarization per spike. These effects cause the train of after-discharges to terminate at a depolarized membrane potential. The value of this potential is not dominated by the reversal potential for K^+. The inward current, conducted by the noninactivating fraction of Na^+ channels, is large enough to shift the equilibrium potential to a depolarized value relative to E_K. Therefore, the small shift in E_K caused by T-tubular K^+ accumulation depolarizes the membrane sufficiently to activate Na^+ channels, but it is primarily the magnitude of the persistent Na^+ current that generates the large depolarizing shift in the resting potential. From this depolarized state, the vast majority of Na^+ channels are inactivated. Consequently, the cell is unable to generate an action potential in response to subsequent stimuli (Fig. 11 *C*). This refractory state is the model homologue of flaccid paralysis that occurs in combination with a large depolarizing shift of the resting potential (Rüdel and Lehmann-Horn, 1985). Thus, the defects of Na^+ channel inactivation observed in T1313M are predicted to cause myotonia that may progress to paralysis.

We propose that a consistent pattern is emerging between the particular type of Na^+ channel inactivation defect and the clinical phenotype. A depolarizing shift in $h_\infty(V)$ predisposes to myotonia, whereas an increase in the noninactivating fraction of Na^+ channels, f, usually leads to weakness from depolarization block of action potential generation. Model simulations were performed to examine the sensitivity of the system to changes in the midpoint of $h_\infty(V)$ or in the magnitude of f, when 50% of the channels were WT and the other half were modified. A 4-mV depolarizing shift of $h_\infty(V)$ was sufficient to produce multiple spikes during a maintained stimulus of 1.5× threshold intensity. Myotonic responses, without the development of a stable depolarized V_{rest}, were generated when $V_{1/2}$ was shifted rightward over a range from 4 to 18 mV. Larger shifts in $V_{1/2}$ caused long trains of myotonic discharges that

slowly decayed to a depolarized V_{rest}. Mutations in R1448 of the IVS4 segment cause myotonia and yet shift the $h_\infty(V)$ curve in the hyperpolarizing direction (Chahine et al., 1994). Simulations show that the change in steady-state inactivation still causes myotonia because these mutations reduce the slope of $h_\infty(V)$, which enhances excitability by producing a larger window current. In contrast to this large range of shifts in $h_\infty(V)$ that produce myotonia, an increase in f caused myotonic responses over only a narrow range, 0.008–0.02. With slightly higher fractions of noninactivating Na^+ current, a brief burst of discharges decayed to a depolarized V_{rest} (Fig. 11 *C*). Still higher values of f caused stable depolarization block after a single spike.

Conclusions from the model simulation are substantiated by genotype–phenotype correlations. When a mutation causes a large persistent Na^+ current (>2% of peak), attacks of weakness are usually a prominent clinical feature. Large noninactivating Na^+ currents have been observed with the following mutations: the two most commonly occurring mutations that cause hyperkalemic periodic paralysis, T704M and M1592V (Cannon and Strittmatter, 1993), one variant of PMC with weakness, T1313M (this study), and an equine form of K^+-aggravated periodic paralysis, equivalent to F1419L (Cannon et al., 1995). These mutations may also slow $\tau_h(V)$ and shift the voltage dependence of $h_\infty(V)$. Conversely, myotonic disorders without concomitant weakness are associated with Na^+ channel mutations that slow τ_h and shift $h_\infty(V)$ but do not cause a large persistent Na^+ current. The small window current resulting from a shifted $h_\infty(V)$ provides a destabilizing influence and leads to repetitive firing but is not sufficient to produce a stable depolarized shift in the resting potential. A slowed τ_h also favors repetitive firing. Mutations that produce this type of inactivation defect include: the SCM-associated mutations at G1306A/V/E (this study) and PMC without weakness at L1433R (Chahine et al., 1994, Yang et al., 1994). Lerche et al. (1993) have commented that the size and charge of the residue at G1306 (A < V < E) correlates with the magnitude of the persistent current and the clinical severity of myotonia. Although our data are consistent with this rank order in terms of the $V_{1/2}$ shift for $h_\infty(V)$, the model simulations suggest that the small differences in τ_h, $h_\infty(V)$, and I_{ss}/I_{pk} may not be sufficient to account for the phenotypic variability. G1306A causes myotonia fluctuans, a relatively mild form of myotonia triggered by rest after exercise or oral potassium loading. G1306V is associated with moderate, exercise-induced myotonic stiffness. G1306E causes myotonia permanens, a severe constant myotonia that may impair breathing (because of hyperactive stiffness rather than weakness) and require treatment with Na^+ channel blockers.

Exceptions to this scheme have been reported, but these are difficult to interpret because the clinical descriptions are often incomplete or conflicting for the same mutation; furthermore, it is difficult to unequivocally detect small persistent Na^+ currents (2–5% of peak) from whole-cell recordings. One exception is V1589M, which is associated with K^+-aggravated myotonia without weakness, and yet had a steady-state current 3.5% of the peak (Mitrovic et al., 1994). R1448C and R1448H both cause PMC with weakness, but whole-cell recordings did not show large persistent currents (Chahine et al., 1994, Yang et al., 1994) although neither study provided quantified values of I_{ss}/I_{pk}.

The mechanisms underlying sensitivity to extracellular $[K^+]$, delayed-onset myotonia after exercise, and phenotypic variation within members of a single affected family are not well understood. The possibility that raised extracellular K^+ directly alters gating of mutant Na^+ channels in hyperkalemic periodic paralysis has been suggested by two of our previous studies (Cannon et al., 1991; Cannon et al., 1995). In both cases, unitary currents were recorded from cultured myotubes. Heterologous expression of one of these mutants (M1592V) in HEK cells did produce Na^+ currents with a large noninactivating component, but there was no consistent K^+ sensitivity of the defect (Cannon and Strittmatter, 1993). One possible explanation for the discrepancy is the absence of the β_1 subunit in those experiments. In the present study, α and β_1 subunit cDNAs were cotransfected into HEK cells. For heteromeric Na^+ channels, a fourfold rise in external $[K^+]$ caused a mild, voltage-independent slowing of inactivation (τ_h) for both G1306E and WT channels. The fractional steady-state current, however, was increased by elevated $[K^+]_o$ for G1306E but not WT channels. These effects were small, but the changes were in the correct direction to aggravate myotonia and therefore may contribute to K^+-induced symptoms. In any event, addition of the β_1 subunit does not resolve the discrepancy between the presence of K^+ effects in myotubes and their absence in heterologous expression systems. The most prominent effect of cotransfection with the β_1 subunit was an increase in the Na^+ current density.

A characteristic feature of PMC is a worsening of myotonia by cooling. Because SCM and HyperPP are not substantially exacerbated by cold, it is natural to ask whether the PMC-associated subset of Na^+ channel mutations cause a particularly abnormal temperature sensitivity of channel gating. One mechanism could be that τ_h or P_oss have aberrantly large Q_{10} values so that moderate cooling tremendously slows inactivation or produces a very large persistent Na^+ current. The data do not support this hypothesis. The temperature sensitivity of τ_h is indistinguishable for WT and T1313M (Fig. 9, *B* and *C*), and the cold-induced increase in I_{ss} is less steep for T1313M than for WT (Fig. 9 *D*). One pos-

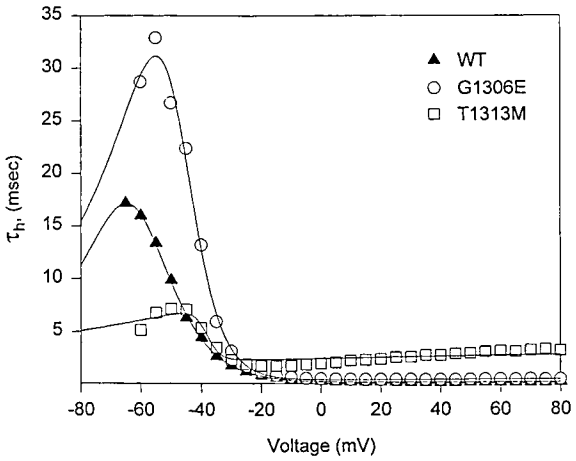

FIGURE 12. Model simulation of altered inactivation kinetics. The time constant of macroscopic current decay, τ_h, is replotted from Fig. 2 *B* on a linear scale. Smooth curves show the fidelity of the simulated Na^+ channel behavior, using the parameter values listed in Table IV.

sible explanation is that the clinical expression of altered muscle function may depend on a threshold effect. Because both I_{ss} and τ_h differ greatly between T1313M and WT even at warm temperatures, mild cooling may cause the value of I_{ss} or τ_h for T1313M, but not for WT, to increase sufficiently to produce myotonia or weakness. While considering the possibility of a threshold mechanism for the temperature dependence of clinical symptoms, it should be noted that the effective Q_{10} for τ_h is quite large at voltages < -10 mV (Fig. 9 *C*). This increase in Q_{10} at hyperpolarized potentials is a reflection that τ_h is strongly dependent on a series of state transitions (activation through closed states) in this voltage range. Conversely, for depolarizations of 0 mV or greater, τ_h is determined primarily by a single transition from the open to inactive state, and this single barrier produces a more typical Q_{10} of 3–3.5. An alternative explanation for the apparent lack of increased temperature sensitivity of the mutant Na^+ channels is that temperature-induced changes in other systems such as Na/K ATPase activity or shifts in reversal potentials may alter the consequences of a gating defect in mutant Na^+ channels and thereby produce the phenotype.

In one regard, all of the Na^+ channel α subunit mutations that cause myotonia or paralysis share a common pathophysiologic mechanism. Every mutation causes an impairment of inactivation that can be viewed as a gain of function, as opposed to a loss of function caused by a mutation that eliminates or reduces Na^+ current. For Na^+ channels, the noninactivating current depolarizes the cell and thereby inactivates all the normally functioning Na^+ channels, which results in a dominant phenotype for these disorders.

APPENDIX

Two changes were made in our previous model of a muscle cell (Cannon et al., 1993) to explore the functional consequences of the mutations in the III–IV loop. First, the kinetics of inactivation were modified to match the behavior of wild-type or mutant channels observed in HEK cells. Second, two populations of Na^+ channels, mutant and WT, were included in the model to simulate the heterozygous state.

As in our previous model, the voltage and temporal dependence of ionic conductances were simulated with the Hodgkin-Huxley formalism. The most convenient method to define the inactivation parameter, $h(V,t)$, to simulate the observed changes in $\tau_h(V)$ and $h_\infty(V)$ was in terms of these two experimentally determined parameters:

$$\frac{dh}{dt} = \frac{h_\infty - h}{\tau_h}$$

The Boltzmann fits listed in Table I (+ β_1 condition) were used to approximate $h_\infty(V)$. Because the voltage dependence of gating is shifted to the right (depolarized) in HEK cells compared with skeletal muscle, the $V_{1/2}$ was shifted in the simulation so that $V_{1/2} = -80$ mV for WT channels, and the relative rightward shift was preserved for G1306E and T1313M (Table I). The standard Hodgkin-Huxley forward, $\alpha_h(V)$, and backward, $\beta_h(V)$, rate relations were used to approximate $\tau_h(V)$. The closeness of the fits are shown in Fig. 12, and the parameter values are listed in Table IV. As was the case for $h_\infty(V)$, the midpoints of the $\tau_h(V)$ fits were shifted to compensate for the difference between HEK cells and skeletal muscle. Finally, the persistent current was simulated by empirically varying the fraction of channels that failed to inactivate, f, until the simulated I_{ss}/I_{pk} matched the observed value listed in Table I. The effective inactivation parameter, $h_{eff}(V)$, was then defined as $h_{eff} = (1 - f)h_\infty + f$.

The total Na^+ current was simulated as a combination of WT and mutant currents. Two constraints were

TABLE IV

Model Parameters for the Simulation

Parameter	WT	G1306E	T1313M	Units
f	0.0015	0.004	0.09	—
$\bar{g}_{Na}$	150	69 (75)*	30 (99)*	mS/cm^2
$V_{1/2}$	−80	−70.3	−62.9	mV
K_h	4.8	5.0	5.0	mV
$\bar{\alpha}_h$	0.00012	0.00048	0.122	ms^{-1}
$K_{\alpha h}$	12.5	12.6	78.5	mV
$\bar{\beta}_h$	6.4	2.4	0.32	ms^{-1}
$K_{\beta h}$	12.3	8.1	2.5	mV
$\bar{V}_h$	−12.6	−28.6	−51.8	mV

*Values in parentheses show the corresponding $\bar{g}_{Na}$ for the WT channels in the simulation of the heterozygous state.

used to simulate this combination: (*a*) The total peak Na^+ current density was kept constant, ~4.2 mA/cm^2; and (*b*) the relative amplitude of each component was adjusted such that I_{WT}/I_{G1036E} was 1:1 and I_{WT}/I_{T1313M} was 2:1. This proportioning of current densities assumes that the expression of G1306E is comparable to that of WT whereas T1313M expresses less efficiently (as shown in the HEK system). The constraints were incorporated into the model by scaling the peak conductance parameter, g_{Na}, for each current type as listed in Table IV.

All other parameter values were identical to those values used by Cannon et al. (1993).

The authors thank David Corey, in whose laboratory some of the physiology experiments were performed, and Adriana Pechanova for assistance with tissue culture.

This work was supported by fellowships from the Howard Hughes Medical Institute (L.J. Hayward and S.C. Cannon), the National Institutes of Health (AR42703, AR41025, and NS07340), the Muscular Dystrophy Association (L.J. Hayward, R.H. Brown, Jr., and S.C. Cannon), the A.P. Sloan Foundation (S.C. Cannon) and the CB Day Co. (R.H. Brown, Jr.).

Original version received 7 September 1995 and accepted version received 2 January 1996.

REFERENCES

Aldrich, R.W., and C.F. Stevens. 1987. Voltage-dependent gating of single sodium channels from mammalian neuroblastoma cells. *J. Neurosci.* 7:418–431.

Armstrong, C.M., and F. Bezanilla. 1977. Inactivation of the sodium channel. II. Gating current experiments. *J. Gen. Physiol.* 70:567–590.

Cannon, S.C., and D.P. Corey. 1993. Loss of Na^+ channel inactivation by anemone toxin (ATX II) mimics the myotonic state in hyperkalemic periodic paralysis. *J. Physiol. (Camb.).* 466:501–520.

Cannon, S.C., and S.M. Strittmatter. 1993. Functional expression of sodium channel mutations identified in families with periodic paralysis. *Neuron.* 10:317–326.

Cannon, S.C., R.H. Brown, and D.P. Corey. 1991. A sodium channel defect in hyperkalemic periodic paralysis: potassium-induced failure of inactivation. *Neuron.* 6:619–626.

Cannon, S.C., R.H. Brown, and D.P. Corey. 1993. Theoretical reconstruction of myotonia and paralysis caused by incomplete inactivation of sodium channels. *Biophys. J.* 65:270–288.

Cannon, S.C., L.J. Hayward, J. Beech, and R.H. Brown, Jr. 1995. Sodium channel inactivation is impaired in equine hyperkalemic periodic paralysis. *J. Neurophysiol. (Bethesda).* 73:1892–1899.

Catterall, W.A. 1992. Cellular and molecular biology of voltage-gated sodium channels. *Physiol. Rev.* 72:S15–S48.

Chahine, M., A.L. George, M. Zhou, S. Ji, W. Sun, R.L. Barchi, and R. Horn. 1994. Sodium channel mutations in paramyotonia congenita uncouple inactivation from activation. *Neuron.* 12:281–294.

Cota, G., and C. Armstrong. 1989. Sodium channel gating in clonal pituitary cells: the inactivation step is not voltage dependent. *J. Gen. Physiol.* 94:213–232.

Cummins, T.R., J. Zhou, F.J. Sigworth, C. Ukomadu, M. Stephan, L.J. Ptácek, and W. Agnew. 1993. Functional consequences of a Na^+ channel mutation causing hyperkalemic periodic paralysis. *Neuron.* 10:667–678.

Deng, W.P., and J.A. Nickoloff. 1992. Site-directed mutagenesis of virtually any plasmid by eliminating a unique site. *Anal. Biochem.* 200:81–88.

Freygang, W.H., D.A. Goldstein, and D.C. Hellam. 1964. The after-potential that follows a train of impulses in frog muscle fibers. *J. Physiol. (Camb.).* 47:929–951.

Heinemann, S., and F. Conti. 1992. Nonstationary noise analysis and application to patch clamp recordings. *Methods Enzymol.* 207: 131–148.

Ho, S.N., H.D. Hunt, R.M. Horton, J.K. Pullen, and L.R. Pease. 1989. Site-directed mutagenesis by overlap extension using the polymerase chain reaction. *Gene (Amst.).* 77:51–59.

Hodgkin, A.L., and A.F. Huxley. 1952. The dual effect of membrane potential on sodium conductance in the giant axon of *Loligo. J. Physiol. (Camb.).* 116:497–506.

Isom, L.L., K.S. DeJongh, D.E. Patton, B.F.X. Reber, J. Offord, H. Charbonneau, K. Walsh, A.L. Goldin, and W.A. Catterall. 1992. Primary structure and functional expression of the β1 subunit of the rat brain sodium channel. *Science (Wash. DC).* 256:839–842.

Jackson, C.E., R.J. Barohn, and L.J. Ptacek. 1994. Paramyotonia congenita: abnormal short exercise test, and improvement after mexiletine therapy. *Muscle & Nerve.* 17:763–768.

Jurman, M.E., L.M. Boland, Y. Liu, and G. Yellen. 1994. Visual identification of individual transfected cells for electrophysiology using antibody-coated beads. *Biotechniques.* 17:874–881.

Kraner, S.D., J.C. Tanaka, and R.L. Barchi. 1985. Purification and functional reconstitution of the voltage-sensitive sodium channel from rabbit T-tubular membranes. *J. Biol. Chem.* 25:6341–6347.

Kuo, C.C., and B.P. Bean. 1994. Na^+ channels must deactivate to recover from inactivation. *Neuron.* 12:819–829.

Lerche, H., R. Heine, U. Pika, A.L. George, Jr., N. Mitrovic, M. Browatzki, T. Weiβ, M. Rivet-Bastide, C. Franke, M. Lomonaco, K. Ricker, and F. Lehmann-Horn. 1993. Human sodium channel myotonia: slowed channel inactivation due to substitutions for a glycine within the III-IV linker. *J. Physiol. (Camb.).* 470:13–22.

McClatchey, A.I., S.C. Cannon, S.A. Slaugenhaupt, and J.F. Gusella. 1993. The cloning and expression of a sodium channel β1-subunit cDNA from human brain. *Hum. Mol. Genet.* 2:745–749.

Mitrovic, N., A.L. George, R. Heine, S. Wagner, U. Pika, U. Hartlaub, M. Zhou, H. Lerche, Ch. Fahlke, and F. Lehmann-Horn. 1994. K^+-aggravated myotonia: destabilization of the inactivated state of the human muscle Na^+ channel by the V1589M mutation. *J. Physiol. (Camb.).* 478:395–402.

Mitrovic, N., A.L. George, H. Lerche, S. Wagner, Ch. Fahlke, and F. Lehmann-Horn. 1995. Different effects on gating of three myotonia-causing mutations in the inactivation gate of the human mus-

cle sodium channel. *J. Physiol. (Camb.).* 487:107–114.

O'Leary, M.E., L.Q. Chen, R.G. Kallen, and R. Horn. 1995. A molecular link between activation and inactivation of sodium channels. *J. Gen. Physiol.* 106:641–658.

Ricker, K., R.T. Moxley, R. Heine, and F. Lehmann-Horn. 1994. Myotonia fluctuans: a third type of muscle sodium channel disease. *Arch. Neurol.* 51:1095–1102.

Riggs, J.E. 1988. The periodic paralyses. *Neurologic Clinics.* 6:485–498.

Rüdel, R., and F. Lehmann-Horn. 1985. Membrane changes in cells from myotonia patients. *Physiol. Rev.* 65:310–356.

Rüdel, R., K. Ricker, and F. Lehmann-Horn. 1993. Genotype-phenotype correlations in human skeletal muscle sodium channel diseases. *Arch. Neurol.* 50:1241–1248.

Sambrook, J., E.F. Fritsch, and T. Maniatis. 1989. Molecular Cloning: A Laboratory Manual. Cold Spring Harbor Press, Cold Spring Harbor, NY.

Sigworth, F.J. 1980. The variance of sodium current fluctuations at the node of Ranvier. *J. Physiol. (Camb.).* 307:97–129.

Stühmer, W., F. Conti, H. Suzuki, X. Wang, M. Noda, N. Yahagi, H. Kubo, and S. Numa. 1989. Structural parts involved in activation and inactivation of the sodium channel. *Nature (Lond.).* 339:597–603.

Tahmoush, A.J., K.L. Schaller, P. Zhang, T. Hyslop, T. Heiman-Patterson, and J.H. Caldwell. 1994. Muscle sodium channel inactivation defect in paramyotonia congenita with the Thr1313Met mutation. *Neuromuscular Disorders.* 4:447–454.

Trimmer, J.S., S.S. Cooperman, S.A. Tomiko, J. Zhou, S.M. Crean, M.B. Boyle, R.G. Kallen, Z. Sheng, R.L. Barchi, F.J. Sigworth, et al. 1989. Primary structure and functional expression of a mammalian skeletal muscle sodium channel. *Neuron.* 3:33–49.

West, J.W., D.E. Patton, T. Scheuer, Y. Wang, A.L. Goldin, and W.A. Catterall. 1992. A cluster of hydrophobic amino acid residues required for fast Na^+ channel inactivation. *Proc. Natl. Acad. Sci. USA.* 89:10910–10914.

Yang, N., S. Ji, M. Zhou, L.J. Ptácek, R.L. Barchi, R. Horn, and A.L. George. 1994. Sodium channel mutations in paramyotonia congenita exhibit similar biophysical phenotypes *in vitro. Proc. Natl. Acad. Sci. USA.* 91:12785–12789.